5444 *Inorg. Chem.* **2010**, *49*, 5444–5452
DOI: 10.1021/ic100185m

Inorganic Chemistry
Article

Synthesis and Structural Studies of Chiral Indium(III) Complexes Supported by Tridentate Diaminophenol Ligands

Alberto Acosta-Ramírez,[†] Amy F. Douglas,[†] Insun Yu,[†] Brian O. Patrick,[†] Paula L. Diaconescu,[‡] and Parisa Mehrkhodavandi*,[†]

[†]*Department of Chemistry, University of British Columbia, 2036 Main Mall, Vancouver, BC, Canada, and*
[‡]*Department of Chemistry & Biochemistry, University of California, Los Angeles, California 90095*

Received January 29, 2010

Indium(III) dimethyl, dihalide, and alkoxy-bridged complexes bearing a chiral diaminophenoxy tridentate ligand $[NN_HO]^-$ were synthesized. The dimethyl complex $(NN_HO)InMe_2$ (**1**) was unreactive toward ethanol and 2-propanol and only partially reactive toward the more acidic phenol. The dihalide complexes $(NN_HO)InX_2$ (X = Cl (**3**), Br (**4**), I (**5**)) reacted with NaOEt to form robust alkoxy-bridged complexes with the formula $\{[(NN_HO)InX]_2(\mu\text{-}X)(\mu\text{-}OEt)\}$ (X = Cl (**6**), Br (**7**), I (**8**)). The reaction of the alkoxy-bridged complexes with water produced hydroxy-bridged dinuclear indium compounds. The hydroxy-bridged complex bearing a chloride ligand $[(NN_HO)InCl(\mu\text{-}OH)]_2$ (**9**) was significantly more reactive toward dissociation and formation of a pyridine adduct than the iodo analogue $[(NN_HO)InI(\mu\text{-}OH)]_2$ (**10**). All compounds were fully characterized in solution by NMR spectroscopy and in the solid state by single-crystal X-ray diffraction. In addition, DFT calculations were used to help explain the reactivity trends observed.

Introduction

Indium(III) has emerged recently as a versatile, functional-group-tolerant Lewis acid in many organic transformations.[1−6] Indium(III) salts have proven to be exceptionally stable toward air and water in numerous applications, traits that have allowed them to gain an edge over metals with similar reactivity (zinc and tin). In addition to the numerous reactions in which indium acts as a stoichiometric reagent, indium(III) salts, in conjunction with chiral ligands, have been used to catalyze enantioselective transformations such as allylations,[7−13] Diels−Alder reactions,[14,15] and formation of homoallylic alcohols.[7,16]

We reported the first indium catalyst for the living polymerization of lactide[17] as part of our efforts to develop active initiators for the controlled ring-opening polymerization of cyclic esters.[18] Prior to our work, an indium catalyst for the polymerization of caprolactone was reported.[19] Subsequently, other indium complexes bearing achiral[20] or chiral ligands,[21] as well as In(III) salts,[22] with good activity and selectivity were reported for the polymerization of lactide.

The emergence of indium as an important Lewis acid catalyst and the relative paucity of indium complexes supported by chiral ligands[21,23−28] emphasize the importance of

*To whom correspondence should be addressed. E-mail: mehr@chem.ubc.ca.

(1) Loh, T. P.; Chua, G. L. *Chem. Commun.* **2006**, 2739–2749.
(2) Frost, C. G.; Hartley, J. P. *Mini-Rev. Org. Chem.* **2004**, *1*, 1–7.
(3) Fringuelli, F.; Piermatti, O.; Pizzo, F.; Vaccaro, L. *Curr. Org. Chem.* **2003**, *7*, 1661–1689.
(4) Chauhan, K. K.; Frost, C. G. *J. Chem. Soc., Perkin Trans.* **2000**, 3015–3019.
(5) Li, C. J.; Chan, T. H. *Tetrahedron* **1999**, *55*, 11149–11176.
(6) Cintas, P. *Synlett* **1995**, 1087–1096.
(7) Lu, J.; Hong, M. L.; Ji, S. J.; Loh, T. P. *Chem. Commun.* **2005**, 1010–1012.
(8) Lu, J.; Hong, M. L.; Ji, S. J.; Teo, Y. C.; Loh, T. P. *Chem. Commun.* **2005**, 4217–4218.
(9) Lu, J.; Ji, S. J.; Loh, T. P. *Chem. Commun.* **2005**, 2345–2347.
(10) Teo, Y. C.; Tan, K. T.; Loh, T. P. *Chem. Commun.* **2005**, 1318–1320.
(11) Lu, J.; Ji, S. J.; Teo, Y. C.; Loh, T. P. *Org. Lett.* **2005**, *7*, 159–161.
(12) Teo, Y. C.; Goh, J. D.; Loh, T. P. *Org. Lett.* **2005**, *7*, 2743–2745.
(13) Zhang, X.; Chen, D. H.; Liu, X. H.; Feng, X. M. *J. Org. Chem.* **2007**, *72*, 5227–5233.
(14) Fu, F.; Teo, Y. C.; Loh, T. P. *Org. Lett.* **2006**, *8*, 5999–6001.
(15) Teo, Y. C.; Loh, T. P. *Org. Lett.* **2005**, *7*, 2539–2541.
(16) Zhao, J. F.; Tsui, H. Y.; Wu, P. J.; Lu, J.; Loh, T. P. *J. Am. Chem. Soc.* **2008**, *130*, 16492–16493.
(17) Douglas, A. F.; Patrick, B. O.; Mehrkhodavandi, P. *Angew. Chem., Int. Ed.* **2008**, *47*, 2290–2293.
(18) Labourdette, G.; Lee, D. J.; Patrick, B. O.; Ezhova, M. B.; Mehrkhodavandi, P. *Organometallics* **2009**, *28*, 1309–1319.
(19) Hsieh, I. P.; Huang, C. H.; Lee, H. M.; Kuo, P. C.; Huang, J. H.; Lee, H. I.; Cheng, J. T.; Lee, G. H. *Inorg. Chim. Acta* **2006**, *359*, 497–504.
(20) Peckermann, I.; Kapelski, A.; Spaniol, T. P.; Okuda, J. *Inorg. Chem.* **2009**, *48*, 5526–5534.
(21) Buffet, J.-C.; Okuda, J.; Arnold, P. L. *Inorg. Chem.* **2010**, *49*, 419–426.
(22) Pietrangelo, A.; Hillmyer, M. A.; Tolman, W. B. *Chem. Commun.* **2009**, 2736–2737.
(23) Schumann, H.; Kaufmann, J.; Wassermann, B. C.; Girgsdies, F.; Jaber, N.; Blum, J. *Z. Anorg. Allg. Chem.* **2002**, *628*, 971–978.
(24) Schumann, H.; Kaufmann, J.; Dechert, S. *Z. Anorg. Allg. Chem.* **2004**, *630*, 1999–2005.
(25) Gao, Q.; Jiang, F. L.; Wu, M. Y.; Huang, Y. G.; Chen, L.; Wei, W.; Hong, M. C. *J. Solid State Chem.* **2009**, *182*, 1499–1505.
(26) Yuan, F.; Zhu, C. J.; Sun, J. T.; Liu, Y. J.; Pan, Y. *J. Organomet. Chem.* **2003**, *682*, 102–107.
(27) Chitsaz, S.; Neumuller, B. *Organometallics* **2001**, *20*, 2338–2343.
(28) Pauls, J.; Chitsaz, S.; Neumuller, B. *Z. Anorg. Allg. Chem.* **2000**, *626*, 2028–2034.

Published on Web 05/18/2010

Scheme 1. Synthesis of Dialkyl Indium Complexes (NN_HO)$InMe_2$ (**1**) and (NN_HO)$InMe_2 \cdot InClMe_2$ (**2**)

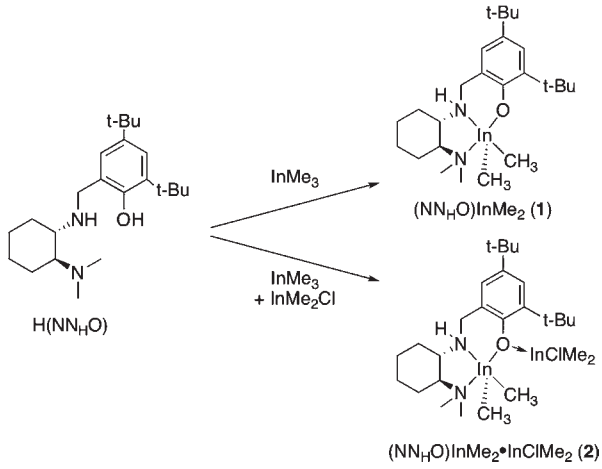

developing well-characterized chiral indium complexes.[29−34] In this work, we present our investigations into the coordination chemistry and structural characteristics of a family of indium(III) complexes supported by a chiral tridentate diaminophenol ligand, H(NN_HO), and provide explanations for the significant halide effect observed in these systems.

Results and Discussion

Synthesis of Indium Alkyl Complexes. Alkyl indium complexes were synthesized via protonolysis reactions between $InMe_3$, either purchased or formed *in situ* from $InCl_3$ and methyllithium,[35] and the proligand H(NN_HO) (Scheme 1).[17,36] With strict control of stoichiometry, the dimethyl species (NN_HO)$InMe_2$ (**1**) was formed as a white solid in a 41% purified yield. When the reaction was carried out using isolated $InMe_3$, complex **1** was obtained in 85% yield. The ^1H NMR spectrum (C_6D_6) of **1** showed characteristic multiplets for the methylene backbone of the coordinated NN_HO at 4.00 and 3.08 ppm, as well as two singlets for the indium-bound methyl groups at 0.12 and −0.03 ppm.

Crystals of **1** suitable for X-ray diffraction were obtained from diethyl ether at −35 °C. The solid-state structure indicated a distorted square-pyramidal geometry around the indium center with the tridentate ligand bound meridionally (Figure 1). The N1−In bond length (2.503(2) Å) is slightly longer than the N2−In distance (2.355(2) Å), likely due to the presence of the sterically hindered tertiary amine. The In−C1 and In−C2 distances, 2.161(2) and 2.150(2) Å, respectively, are similar to those of related methyl indium complexes.[20,35]

Initial attempts to form **1** from $InMe_3$ generated *in situ* resulted in the isolation of the byproduct (NN_HO)$InMe_2 \cdot InClMe_2$ (**2**), likely a result of the reaction between **1** and

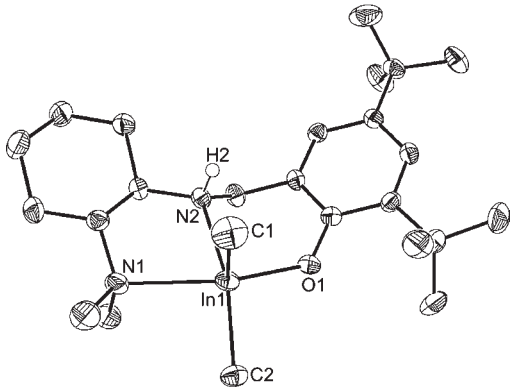

Figure 1. Molecular structure of **1** (depicted with thermal ellipsoids at 50% probability and most H atoms omitted for clarity). Selected bond lengths (Å): N1−In 2.503(2), N2−In 2.3549(18), C1−In 2.161(2), C2−In 2.150(2), O1−In 2.1521(15). Selected bond angles (deg): N1−In−N2 71.20(6), N2−In−O1 80.66(6), O1−In−C2 91.41(8), C2−In−N1 91.15(8), N1−In−C1 100.51(9), N2−In−C1 96.17(9), O1−In−C1 108.15(9), C1−In−C2 127.15(10).

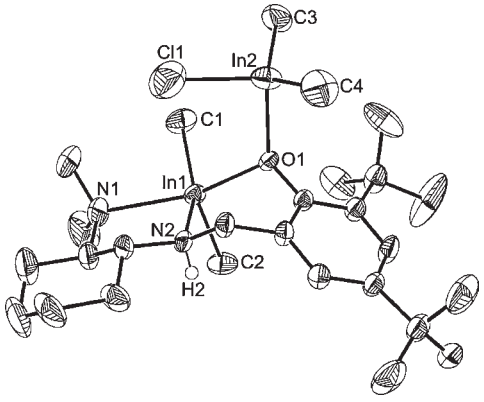

Figure 2. Molecular structure of **2** (depicted with thermal ellipsoids at 50% probability and most H atoms as well as solvent molecules omitted for clarity). Selected bond lengths (Å): N1−In1 2.430(4), N2−In2 2.315(3), O1−In1 2.227(3), O1−In2 2.194(3), C1−In1 2.120(4), C2−In1 2.127(5), C3−In2 2.110(5), C4−In2 2.104(5), Cl−In2 2.3668(18). Selected bond angles (deg): N1−In1−N2 72.25(13), C1−In1−C2 125.2(2), C1−In1−O1 91.46(15), C1−In−N1 92.82(18), C2−In1−O1 104,62(16).

$InClMe_2$, a byproduct of the *in situ* formation of $InMe_3$ with insufficient amounts of methyllithium. The molecular structure of **2** shows a dinuclear complex with $InClMe_2$ coordinated to the phenolic oxygen of **1** (Figure 2). The second metal atom, In(2), has a distorted tetrahedral geometry, while the metal coordinated to the NNO ligand, In(1), has a distorted square-pyramidal geometry, as was observed in the crystal structure of **1**. The distance between In(1) and Cl (3.774 Å) is only slightly larger than the sum of the van der Waals radii for indium and chlorine (3.75 Å).[37]

The dimethylindium complex **1** is generally unreactive or only slightly reactive toward alcohols or bases. Complex **1** does not lose methane when heated in either coordinating (THF) or noncoordinating (toluene) solvents under static vacuum. Attempts to deprotonate the coordinated secondary amine in complex **1** by addition of up to four equivalents of KO(*t*-Bu) and refluxing the mixture in toluene for 48 h did not result in deprotonation

(29) Ziemkowska, W.; Anulewicz-Ostrowska, R. *J. Organomet. Chem.* **2004**, *689*, 2056–2065.
(30) Ziemkowska, W.; Kucharski, S.; Kolodziej, A.; Anulewicz-Ostrowska, R. *J. Organomet. Chem.* **2004**, *689*, 2930–2939.
(31) Ziemkowska, W.; Stella, P.; Anulewicz-Ostrowska, R. *J. Organomet. Chem.* **2005**, *690*, 722–730.
(32) Ullrich, M.; Mitzel, N. W.; Bergander, K.; Frohlich, R. *Dalton Trans.* **2006**, 714–721.
(33) Ziemkowska, W.; Cyranski, M. K. *Organometallics* **2009**, *28*, 5593–5596.
(34) Bösing, P.; Mitzel, N. W. *Dalton Trans.* **2010**, *39*, 66–69.
(35) Zhou, Y. L.; Richeson, D. S. *Organometallics* **1995**, *14*, 3558–3561.
(36) Mitchell, J. M.; Finney, N. S. *Tetrahedron Lett.* **2000**, *41*, 8431–8434.
(37) Batsanov, S. S. *Inorg. Mater.* **2001**, *37*, 871–885.

Scheme 2. Synthesis of Indium Dihalide Complexes $(NN_HO)InX_2$ (X = Cl (**3**), Br (**4**), I (**5**))

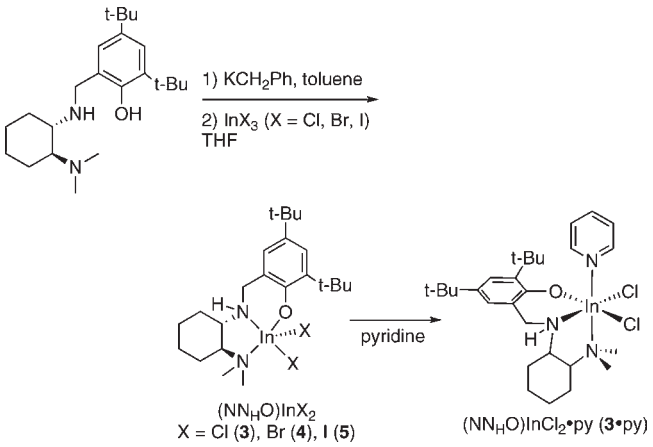

and formation of *t*-BuOH. This lack of reactivity may be due to the low acidity of the secondary amine and/or steric constraints imposed by the geometry of the complex that do not allow the proton of the secondary amine and the methyl group to come close enough to eliminate methane. Complex **1** is also inert toward the addition of one or two equivalents of ethanol or 2-propanol at room temperature or at 60 °C for 12 h. Reactions with phenol show only partial conversion even when a 30-fold excess of phenol is used. When the reaction was warmed for 2 h at 60 °C, the yield could not be improved and only decomposition of the complex was observed. Attempts to isolate the phenoxy complex from the reaction mixture were unsuccessful.[20]

Synthesis of Indium Dihalide Complexes. A salt metathesis route is used to synthesize the indium dihalide complexes $(NN_HO)InX_2$ (X = Cl (**3**), Br (**4**), I (**5**)) (Scheme 2).[17] Various bases such as *n*-butyllithium, potassium hydride, and benzylpotassium were used to deprotonate the proligand $H(NN_HO)$; however, in all cases, only the monodeprotonated form, $[NN_HO]^-$, was isolated. Although secondary amines such as the one present in $H(NN_HO)$ have pK_a values below that of toluene in our chosen solvent, we have never observed deprotonation of the central amine in this or similar systems.[18] The weak acidity of the secondary amine may be due to a hydrogen-bonded six-membered ring, which is formed upon deprotonation of the phenol. This "proton-sponge effect" may increase the stability of the monodeprotonated form and cause a lower acidity of the secondary amine.[38]

The reaction of the potassium salt $K[NN_HO]$ with $InCl_3$ in toluene, at room temperature, for 2 h, forms $(NN_HO)InCl_2$ (**3**) in good yield. When the reaction is conducted in weakly coordinating or noncoordinating solvents, such as diethyl ether or toluene, multiple products are observed by ^{1}H NMR spectroscopy. However, when the reaction is carried out in THF or pyridine, only one isomer of the product is obtained. In both cases, one molecule of THF or pyridine is coordinated to the indium center, as assessed by ^{1}H NMR spectroscopy. While the THF adduct of **3** can lose THF *in vacuo*, the pyridine adduct $(NN_HO)InCl_2\cdot$py (**3**·py) is stable and shows one

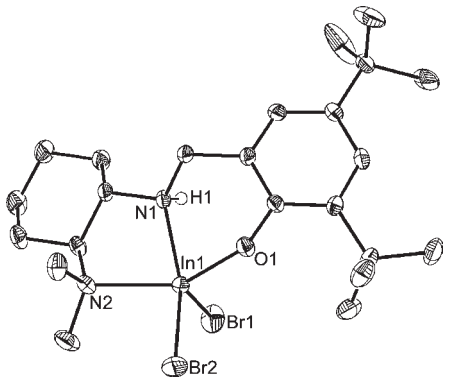

Figure 3. Molecular structure of **4** (depicted with ellipsoids at 50% probability and most H atoms as well as solvent molecules omitted for clarity). Selected bond lengths (Å): N1−In 2.2996(18), N2−In 2.2974(18), O1−In 2.0563(15), In−Br1 2.5123(4), In−Br2 2.5428(3). Selected bond angles (deg): Br1−In−Br2 111.418(13), N1−In−Br2 154.37(5), N2−In−Br2 91.65(5), O1−In−Br2 90.20(4), N1−In−Br1 93.55(5), N1−In−N2 76.96(6), N1−In−O1 85.73(6).

pyridine molecule coordinated in solution and in the solid state. We have reported the molecular structure of **3**·py as a pseudo-octahedral indium center with the tridentate ligand bound in a facial fashion, the two chloride ligands in *cis*-geometry, and the coordinated pyridine *trans* to the dimethylamine moiety.[17]

When a similar salt metathesis reaction is carried out with $InBr_3$ or InI_3 in THF, only the THF-free indium dihalide complexes $(NN_HO)InBr_2$ (**4**) and $(NN_HO)InI_2$ (**5**) are formed. The ^{1}H NMR spectra (CD_2Cl_2) of **4** and **5** show the resonances of the diastereotopic methylene protons in the tridentate ligand ($NHCH_2Ar$) at 4.15 and 4.06 ppm for **4** and 4.14 and 3.98 ppm for **5**. The molecular structure of **4**, obtained by single-crystal X-ray diffraction, shows a distorted square-pyramidal geometry around the indium center, where the apical position is occupied by a bromide ligand (Figure 3). The In−Br bond lengths are in the range reported for similar complexes, with the equatorial In−Br2 (2.5428(3) Å) being slightly longer than the axial In−Br1 bond (2.5123(4) Å).[39]

In order to understand the different reactivity behavior toward adduct formation of the three halides, DFT calculations were used to obtain thermodynamic parameters for the transformation $(NN_HO)InX_2$ + py → $(NN_HO)InX_2$(py). Although this reaction was not experimentally followed for all three halide complexes, the structure of $(NN_HO)InCl_2$(py) could be used for geometry optimizations. The energy of formation for $(NN_HO)InCl_2$(py), although small (−0.2 kcal/mol), indicates that $(NN_HO)InCl_2$(py) is favored, while for $(NN_HO)InBr_2$(py) (3.7 kcal/mol) and $(NN_HO)InI_2$(py) (4.5 kcal/mol), their energies of formation indicate that the adduct is not favored.

Synthesis of Dinuclear Halide/Ethoxy-Bridged Indium Complexes. We have previously reported the one-pot synthesis of $\{[(NNO)InCl]_2(\mu\text{-Cl})(\mu\text{-OEt})\}$ (**6**) via the reaction of (±)-$H(NN_HO)$ with two equivalents of KCH_2Ph, which forms (±)-$K(NN_HO)$ and KOEt, followed by addition to a THF solution of $InCl_3$.[17] Alternatively, the reaction of **3** with one equivalent of sodium ethoxide

(38) Schlosser, M. Organoalkali Chemistry. In *Organometallic in Synthesis: A Manual*, 2nd ed.; M., S., Ed. Wiley: West Sussex, 2002; p 292.

(39) Gurnani, C.; Jura, M.; Levason, W.; Ratnani, R.; Reid, G.; Webster, M. *Dalton Trans.* **2009**, 1611–1619.

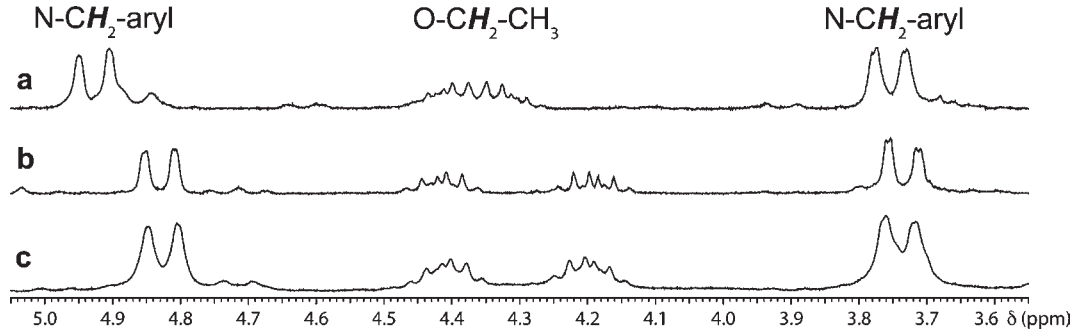

Figure 4. ^{1}H NMR (CD_2Cl_2) resonances for ArCH_2NH and OCH_2CH$_3$ in (a) **6**, (b) **7**, and (c) **8**.

Scheme 3. Synthesis of Dinuclear Complexes {[(NN$_H$O)InX]$_2$(μ-X)(μ-OEt)} (X = Cl (**6**), Br (**7**), I (**8**))

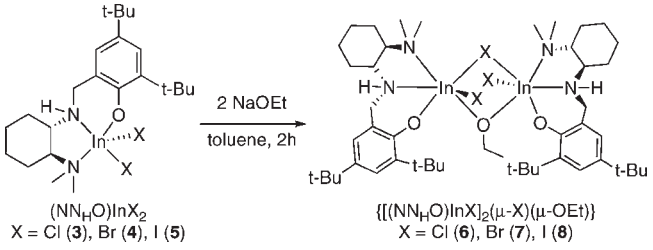

forms the complex (±)-**6** in 67% overall yield based on H(NN$_H$O) (Scheme 3). The molecular structure of **6**, reported previously, shows chloride and ethoxide ligands bridging two indium atoms.[17] Each indium center has a pseudo-octahedral geometry, and the ancillary ligand is facially bound. Although the compound was formed from a racemic mixture of the proligand, only homochiral complexes were observed in the crystal lattice. The ^{1}H NMR spectrum (CD_2Cl_2) shows only one set of peaks for the ancillary ligand. The diastereotopic methylene protons (ArNCH_2) appear at 4.93 and 3.75 ppm, and the resonances for the methylene protons of OCH_2CH$_3$ appear as overlapped multiplets at 4.38 ppm (Figure 4a). The ^{13}C{^{1}H} NMR spectrum also shows only one set of signals. When the enantiopure (*R*,*R*)-H(NN$_H$O) is used to synthesize (*R*,*R*)-**6**, identical NMR chemical shifts are observed. The reaction of **3** with excess NaOEt under more forcing conditions does not proceed further.

In analogous reactions, complexes **4** and **5** react with NaOEt to form the dinuclear complexes {[(NN$_H$O)InX]$_2$(μ-X)(μ-OEt)}, X = Br (**7**), X = I (**8**) (Scheme 3). Using a 2-fold excess of NaOEt or warming the reaction to 60 °C in toluene does not result in the formation of mononuclear complexes. The ^{1}H NMR spectrum (CD_2Cl_2) of **7** shows two characteristic multiplets at 4.40 and 4.19 ppm for the diastereotopic protons of OCH_2CH$_3$ (Figure 4b), while the analogous complex **8** shows two multiplets at 4.40 and 4.21 ppm for the same protons (Figure 4c). The ethoxy-methyl protons resonate at 1.36 and 1.41 ppm for **7** and **8**, respectively. The nonequivalent protons for the ArCH_2NH moiety appear at 4.81 and 3.72 ppm and at 4.83 and 3.75 ppm for **7** and **8**, respectively.

The dinuclear complex **6** is robust and does not dissociate readily in toluene or THF, even at elevated temperatures for 48 h. When excess pyridine is added to a solution of **6** in $CDCl_3$, however, new species were detected by ^{1}H NMR spectroscopy. These are, most likely, different pyridine coordination isomers of (NN$_H$O)InCl$_2$ and (NN$_H$O)InCl(OEt), as evidenced by broad resonances for the pyridine protons observed at 8.90, 7.75, and 7.34 ppm.[40] Similar behavior was observed in CD_2Cl_2 for an analogous reaction with the iodo-bridged complex **8** and two equivalents of pyridine.

Decomposition of the Indium Complexes. A solution of the dinuclear complex **6** is stable at room temperature under an inert atmosphere in different solvents. However, upon exposure to water, **6** rapidly transforms to a hydroxy-bridged complex, [(NN$_H$O)InCl(μ-OH)]$_2$ (**9**) (Scheme 4). A similar reaction was observed with the iodo-bridged analogue **8** to form [(NN$_H$O)InI(μ-OH)]$_2$ (**10**). The ^{1}H NMR spectrum of **10** (benzene-d_6) is similar to that of **9**[17] and shows the diastereotopic NCH_2Ar protons of the ligand at 4.77 and 3.72 ppm and the N(CH_3)$_2$ protons at 2.54 and 1.93 ppm. Most importantly, the characteristic methylene signals for the bridging alkoxy group (OCH_2CH$_3$) are missing. Resonances for the bridging O*H* protons appear as a broad signal at 3.87 ppm.

The solid-state structure of **10** was obtained by single-crystal X-ray diffraction (Figure 5). The structure shows each octahedral indium center with a facially coordinated ancillary ligand, one iodo, and two bridging hydroxy ligands, similar to that obtained for **9**. The In−I bond length is shorter (2.8024(2) Å) than those reported for related octahedral indium complexes (2.9124(6) and 2.9362(5) Å).[41] The bromo analogue (**7**) forms an analogous hydroxy-bridged complex, which was not isolated.

A similar reaction of complex **3** with adventitious water resulted in the isolation of crystals of {[(NN$_H$O)InCl]$_2$(μ-Cl)(μ-OH)} (**11**) (Figure 6). In **11**, the two metal atoms are bound by facially coordinated ligands in a pseudo-octahedral geometry. The structure is similar to that of the dinuclear complex **3**. This type of structure may be a possible intermediate in the conversion of **6** to **9**. A rational synthesis for this complex was not developed.

The hydroxy-bridged complexes **9** and **10** are robust and resist dissociation in the presence of polar solvents such as THF. When two equivalents of pyridine are added to a solution of **9** in $CDCl_3$, several new species were observed in the ^{1}H NMR spectrum. As discussed above, the shifted resonances for pyridine (8.78, 7.72, and 7.33 ppm) suggest the presence of pyridine coordination isomers (NN$_H$O)InCl(OH)(py).[40] Interestingly, when a parallel experiment is

(40) The ^{1}H NMR resonances for free pyridine in $CDCl_3$ appear at 8.62, 7.68, and 7.29 ppm, and those for pyridine in CD_2Cl_2 appear at 8.62, 7.68, and 7.29 ppm.

(41) Cheng, F.; Friend, S. I.; Hector, A. L.; Levason, W.; Reid, G.; Webster, M.; Zhang, W. J. *Inorg. Chem.* **2008**, *47*, 9691–9700.

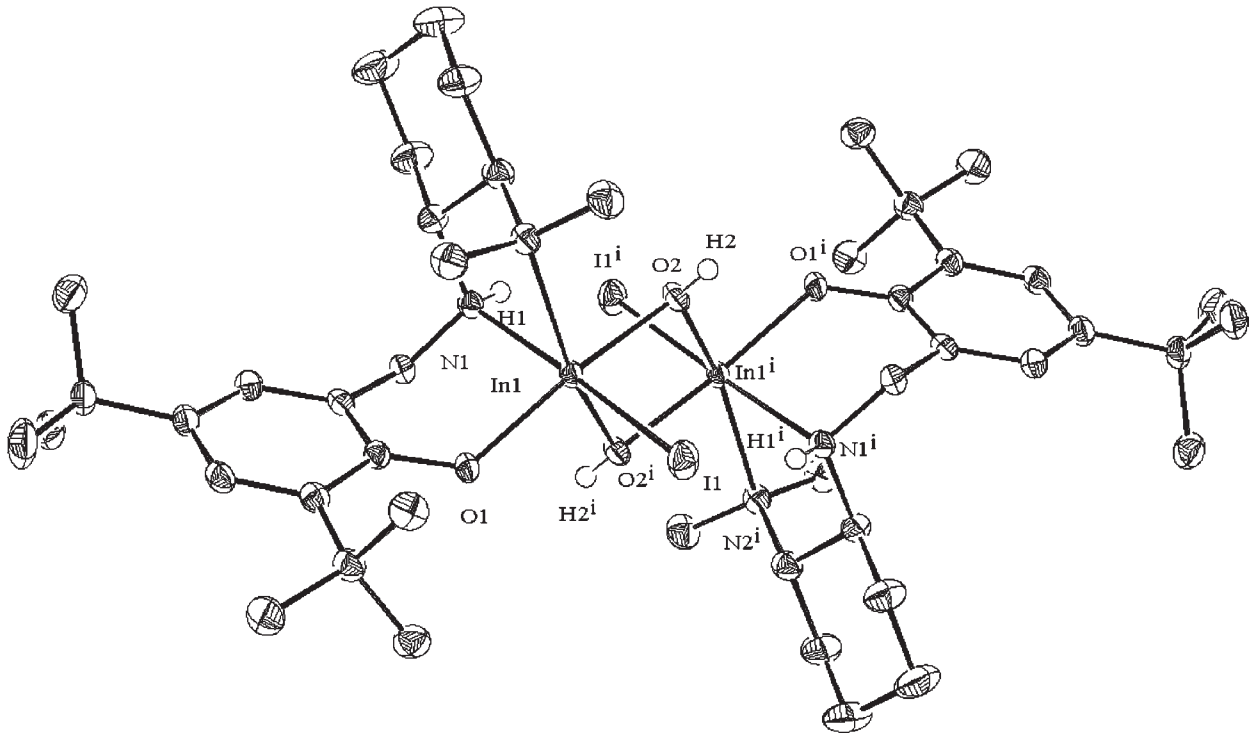

Figure 5. Molecular structure of **10** (depicted with ellipsoids at 50% probability and most H atoms as well as solvent molecules omitted for clarity). Selected bond lengths (Å): N1−In1 2.2855(16), N2−In1 2.3788(16), O1−In1 2.0908(12), O2−In1 2.1402(14), O2−In1^{i} 2.1533(14), In1−O2^{i} 2.1533(14), In1−I 2.8024(2). Selected bond angles (deg): O1−In1−O2 166.06(5), O1−In1−O2^{i} 92.58(5), O2−In1−O2^{i} 74.03(6), O1−In1−N1 86.51(5), O2−In1−N1 89.35(6), O1−In1−N2 103.15(5), O2−In1−N2 88.65(5), N1−In1−N2 75.25(6), O1−In1−I 89.18(4), O2−In1−I 96.35(4), N1−In1−I 172.07(4), N2−In1−I 99.31(4).

Scheme 4. Formation of Dinuclear Complexes $[(NN_HO)InX(\mu\text{-}OH)]_2$ (X = Cl (**9**), I (**10**))

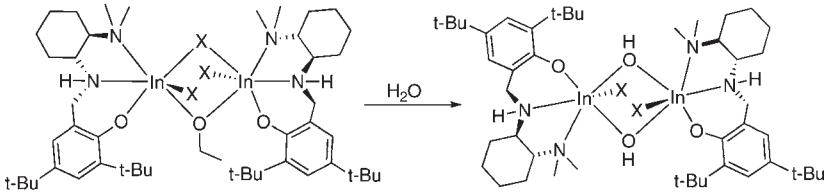

carried out with the iodo-bridged complex **10**, no reaction is observed even after 3 h at room temperature. Dissociation is only observed when **10** is dissolved in neat pyridine for 8 h.

DFT Calculations. DFT calculations were carried out with ADF2009.01[42−44] in order to understand the different reactivity of the various halide analogues for the same type of complex. Calculations were performed on full molecules for the mononuclear complexes and on model compounds in which the *tert*-butyl substituents of the aromatic rings were replaced by methyl groups for economy for the dinuclear complexes. The results of the geometry optimizations indicated that the models showed similar metrical parameters to those obtained from the X-ray crystal structures of **4**, **3**·py, and **10** (Table 1).

Once the validity of the calculations was established, calculations were carried out on the dichloride and diiodido analogues of **4**, on the chloro analogue of **10**, and on models for the ethoxy-bridged complexes **6**−**8**. For each series of complexes, Hirshfeld and Bader charges were calculated using a COSMO solvation model (pyridine for **3**−**5**, CH_2Cl_2 for **6**−**8**, and $CHCl_3$ for **9** and **10**, Table 2). Bader charges[45,46] are considered to be a good indicator of the "real" charge of an atom in a molecule and take into account both ionic and covalent contributions, while Hirshfeld charges are recognized to be less dependent on the optimization parameters employed in calculations.[47−49] These charges explain the observed

(42) *ADF2008.01*; SCM; http://www.scm.com: Theoretical Chemistry, Vrije Universiteit: Amsterdam, The Netherlands.
(43) Guerra, C. F.; Snijders, J. G.; te Velde, G.; Baerends, E. J. *Theor. Chem. Acc.* **1998**, *99*, 391–403.
(44) Velde, G. T.; Bickelhaupt, F. M.; Baerends, E. J.; Guerra, C. F.; Van Gisbergen, S. J. A.; Snijders, J. G.; Ziegler, T. *J. Comput. Chem.* **2001**, *22*, 931–967.
(45) Rodriguez, J. I.; Bader, R. F. W.; Ayers, P. W.; Michel, C.; Gotz, A. W.; Bo, C. *Chem. Phys. Lett.* **2009**, *472*, 149–152.
(46) Rodriguez, J. I.; Koster, A. M.; Ayers, P. W.; Santos-Valle, A.; Vela, A.; Merino, G. *J. Comput. Chem.* **2009**, *30*, 1082–1092.
(47) Guerra, C. F.; Handgraaf, J. W.; Baerends, E. J.; Bickelhaupt, F. M. *J. Comput. Chem.* **2004**, *25*, 189–210.
(48) Du, J. C.; Corrales, L. R. *J. Phys. Chem. B* **2006**, *110*, 22346–22352.
(49) Volkov, A.; Koritsanszky, T.; Chodkiewicz, M.; King, H. F. *J. Comput. Chem.* **2009**, *30*, 1379–1391.

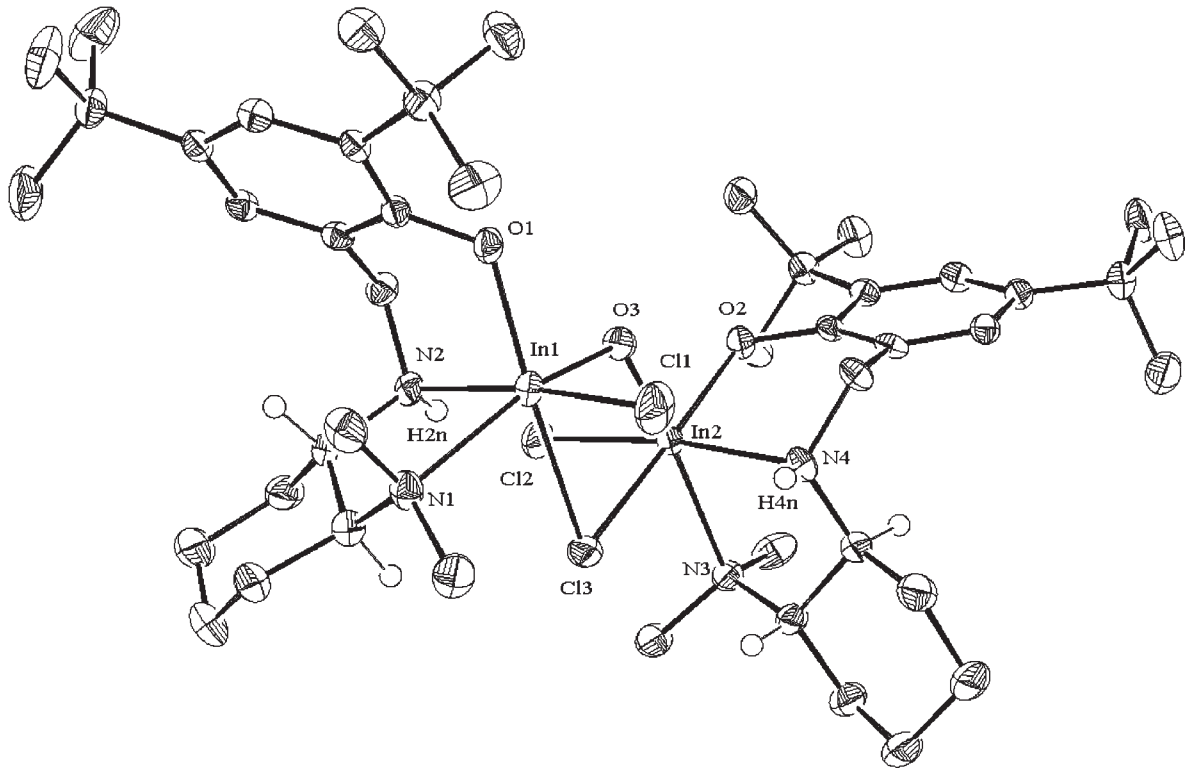

Figure 6. Molecular structure of **11** (depicted with ellipsoids at 50% probability and most H atoms as well as solvent molecules omitted for clarity). Selected bond lengths (Å): N1−In1 2.359(3), N2−In1 2.255(3), N3−In3 2.324(2), N4−In2 2.260(3), O1−In1 2.086(2), O2−In2 2.074(2), O3−In2 2.113(2), O3−In1 2.125(2), In1−Cl1 2.4084(9), In2−Cl2 2.4226(9), In2−Cl3 2.6657(8), In1−Cl3 2.6904(8). Selected bond angles (deg): O1−In1−N1 104.41(9), N1−In1−N2 76.04(9), O1−In−Cl1 95.84(6), In1−Cl31−In2 86.97(2), In1−O3−In2 120.84(9), O2−In2−N4 88.16(9), N3−In2−Cl2 94.97(7).

Table 1. Comparison of Metrical Parameters from Calculated (ADF, gas phase) and X-ray Crystal Structures (experimental) for **4** and **10**

Complex	Parameter	ADF	Experimental
4 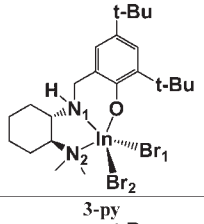	In−N1	2.39 Å	2.30 Å
	In−N2	2.47 Å	2.30 Å
	In−Br1	2.58 Å	2.51 Å
	In-Br2	2.58 Å	2.54 Å
	In-O	2.11 Å	2.06 Å
	Br1InBr2	114.2°	111.4°
	N1InBr1	92.7°	93.5°
	N2InBr2	89.7	91.6°
	N1InN2	73.4°	77.0°
3-py 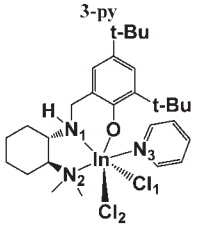	In−N1	2.34 Å	2.27 Å
	In−N2	2.42 Å	2.34 Å
	In-N3	2.40 Å	2.31 Å
	In−Cl1	2.45 Å	2.40 Å
	In-Cl2	2.56 Å	2.52 Å
	In-O	2.18 Å	2.12 Å
	Cl1InCl2	85.3°	86.3°
	N3InCl1	93.3°	93.6°
	N3InCl2	85.3°	86.3°
	N1InN2	75.8°	77.6°
	OInN3	83.4°	84.1°
10 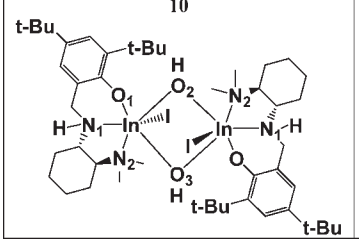	In−N1	2.32 Å	2.29 Å
	In−N2	2.44 Å	2.38 Å
	In−O1	2.15 Å	2.09 Å
	In-O2	2.22 Å	2.14 Å
	In-O3	2.24 Å	2.15 Å
	O1InO2	170.4°	166.1°
	O1InO3	93.9°	92.6°
	N1InI	172.4°	172.1°
	N1InN2	76.0°	72.2°

changes in the reactivity behavior from the chloride to the iodide complexes. A comparison of the indium and halide charges agrees with the reactivity trends observed and described above. In all cases, both the Hirshfeld and the Bader charges of the indium center decrease from the chloro to the bromo and to the iodo complex, while the

Table 2. Calculated Parameters for the Studied Complexes

complex	In Hirshfeld charge	In Bader charge	halide Hirshfeld charge	halide Bader charge
3	0.53	1.59	−0.34 and −0.34	−0.66 and −0.66
4	0.5	1.46	−0.31 and −0.3	−0.58 and −0.58
5	0.44	1.26	−0.25 and −0.24	−0.47 and −0.46
6	0.53 and 0.53	1.67 and 1.67	−0.37 and −0.3 and −0.21	−0.68 and −0.67 and −0.65
7	0.51 and 0.50	1.60 and 1.57	−0.31 and −0.3 and −0.1	−0.62 and −0.6 and −0.53
8	0.47 and 0.46	1.53 and 1.51	−0.26 and −0.25 and −0.08	−0.55 and −0.51 and −0.4
9	0.54	1.72	−0.34	−0.69
10	0.51	1.61	−0.27	−0.57

charges of the halides follow the opposite trend (Table 2). These tendencies can be related to the higher reactivity of the chloride, rather than bromide and iodide, complexes in all series.

Conclusions

A new family of chiral indium alkyl and halide complexes was synthesized and the reactivity of these complexes was studied. The dimethyl complexes did not react with alkyl alcohols; however, incomplete protonolysis reactions were observed with phenol. This reactivity suggests that the protonolysis requires a more acidic alcohol.[18]

The reactivity of the dihalide complexes was strongly dependent on the halide. The more electropositive metal center in the indium dichloride complex **3** reacted with coordinating solvents such as THF to form hexacoordinate species, while the dibromide and the diiodide derivatives were obtained as solvent-free molecules in solution and in the solid state. The dihalide complexes reacted with sodium ethoxide to form robust dinuclear entities with halide and alkoxy-bridging ligands. These molecules dissociated only in the presence of strong donors such as pyridine to form a mixture of coordination isomers in solution. The dinuclear complexes were quantitatively hydrolyzed to stable hydroxy-bridged dinuclear complexes in the presence of water. The dissociation of these compounds also depends on the donor ability of the coordinated halide: the chloro-hydroxy complexes readily dissociated in the presence of pyridine, while the iodo analogues required more forcing conditions. DFT calculations support these observations and show higher positive charges for the indium centers of chloride complexes compared to the bromide or iodide analogues.

Our systematic study of the chiral indium complexes has demonstrated the subtle yet important effect of halide ligands on the nucleophilicity of the indium center. We aim to utilize this knowledge in the development of future indium catalysts for lactide polymerization.

Experimental Section

General Considerations. Unless otherwise indicated, all air- and/or water-sensitive reactions were carried out under dry nitrogen using either an MBraun glovebox or standard Schlenk line techniques. NMR spectra were recorded on a Bruker Avance 400 MHz spectrometer. ^{1}H NMR chemical shifts are reported in ppm versus residual protons in deuterated solvents as follows: δ 7.27 $CDCl_3$, δ 7.16 C_6D_6, δ 5.32 CD_2Cl_2. $^{13}C\{^1H\}$ NMR chemical shifts are reported in ppm versus residual ^{13}C in solvents as follows: δ 77.2 $CDCl_3$, δ 128.4 C_6D_6, δ 54.0 CD_2Cl_2. Diffraction measurements for X-ray crystallography were made on a Bruker X8 APEX II diffractometer with graphite-monochromated Mo Kα radiation. The structures (Table 1) were solved by direct methods and refined by full-matrix least-squares using the SHELXTL crystallographic software of Bruker-AXS. Unless specified, all non-hydrogen atoms were refined with anisotropic displacement parameters, and all hydrogen atoms were constrained to geometrically calculated positions but were not refined. EA CHN analysis was performed using a Carlo Erba EA1108 elemental analyzer. The elemental composition of unknown samples is determined by using a calibration factor. The calibration factor is determined by analyzing a suitable certified organic standard (OAS) of known elemental composition.

Materials. Solvents (pentane, THF, toluene, dichloromethane, and diethyl ether) were degassed and dried using 3 Å molecular sieves in an MBraun Solvent Purification System. THF was further dried over sodium benzophenone ketyl and distilled under N_2. CD_2Cl_2 and $CDCl_3$ were dried over CaH_2 and degassed through a series of freeze−pump−thaw cycles. C_6D_6 was dried over sodium and degassed using a series of freeze−pump−thaw cycles. $InCl_3$, $InBr_3$, InI_3, and $In(Me)_3$ were purchased from Strem Chemicals and used without further purification. For the enantiopure catalyst, (±)-*trans*-1,2-diaminocyclohexane was resolved using Jacobsen's method[50] and then carried forward through the same procedures as used for the *rac*-catalyst. Benzyl potassium was synthesized using a modified literature procedure using *n*-butyllithium (Aldrich), potassium *tert*-butoxide (Alfa Aesar), and toluene.[51] All other compounds were obtained from Aldrich and used without further purification. The literature preparation of H_2NNO[36] was modified as follows: the imine was recrystallized from warm acetonitrile, and the proligand was recrystallized from acetonitrile when it was formed.[17] $K(NN_HO)$ was prepared according to previously reported procedures.[18]

(NN_HO)InMe$_2$ (1). A 125 mL round-bottom flask was charged with $InCl_3$ (0.100 g, 0.45 mmol) and 15 mL of Et_2O. To this solution was added dropwise MeLi in Et_2O (1.6 M, 0.85 mL, 0.45 mmol), and the resulting mixture was stirred at room temperature for 20 min. The proligand H_2NN_HO (0.163 g, 0.45 mmol) was added to the mixture as a solution in Et_2O (15 mL). The reaction was heated at 30 °C for 24 h, after which time it was cooled to room temperature and the solution was filtered through Celite to remove LiCl. The filtrate was concentrated to approximately 15 mL, resulting in the formation of a white precipitate, which was isolated by filtration, washed with pentane (3 × 2 mL), and dried under high vacuum to yield **1** (0.092 g, 41%). Suitable crystals for X-ray diffraction were grown from Et_2O at −35 °C.

Complex **1** can also be synthesized from isolated $In(Me)_3$. A 25 mL round-bottom flask was charged with $In(Me)_3$ (0.071 g, 0.44 mmol) dissolved in 5 mL of Et_2O. Then a solution of the proligand (0.150 g, 0.44 mmol) in 5 mL of Et_2O was added dropwise. The reaction mixture was stirred for 30 min. After the removal of all volatiles the residue was dried *in vacuo*, to yield complex **1** as a white powder (0.188 g, 85%). ^{1}H NMR (400 MHz, $CDCl_3$): δ 7.22 (1H, d, J = 3 Hz, Ar*H*), 6.82 (1H, d, J = 3 Hz, Ar*H*), 4.31 (1H, t, J = 10 Hz, R_2N-C*H*-CH_2), 3.59 (1H, d, J = 7 Hz, NH-CH_2-Ar) 2.61 (1H, d, J = 12 Hz, NH-CH_2-Ar),

(50) Larrow, J. F.; Jacobsen, E. N.; Gao, Y.; Hong, Y. P.; Nie, X. Y.; Zepp, C. M. *J. Org. Chem.* **1994**, *59*, 1939–1942.
(51) Schlosse, M.; Hartmann, J. *Angew. Chem., Int. Ed. Engl.* **1973**, *12*, 508–509.

Table 3. Selected Crystallographic Data for Compounds **1**, **2**, **4**, **10**, and **11**

	1	**2**	**4**	**10**	**11**
empirical formula	$C_{25}H_{45}N_2OIn$	$C_{29.5}H_{57}N_2OIn_2Cl$	$C_{23}H_{39}N_2OInBr_2$	$C_{54}H_{100}N_4O_6In_2I_2$	$C_{61}H_{93}N_4O_3In_2Cl_3$
fw	504.45	720.86	634.20	1384.82	1266.38
T (K)	173	173	173	173	173
a (Å)	19.6863(12)	20.904(3)	10.7405(10)	12.6093(5)	11.5642(5)
b (Å)	13.1562(8)	13.314(2)	18.1340(17)	15.3852(7)	16.8754(8)
c (Å)	20.1573(10)	25.413(5)	13.2261(12)	15.9537(7)	18.1223(8)
α (deg)	90	90	90	90	92.263(2)
β (deg)	90	111.765(9)	92.896(5)	102.392(10)	106.473(2)
γ (deg)	90	90	90	90	109.942(2)
volume (Å^3)	5220.68(5)	6569(2)	2572.7(4)	3022.9(2)	3151.5(2)
Z	8	8	4	2	2
cryst syst	orthorhombic	monoclinic	monoclinic	monoclinic	triclinic
space group	*Pbca*	*C*2/*c*	$P2_1/c$	$P2_1/c$	$P\bar{1}$
d_{calc} (g/cm^3)	1.284	1.458	1.637	1.521	1.335
μ(Mo Kα) (cm^{-1})	9.22	15.08	40.41	18.31	9.03
$2\theta_{max}$ (deg)	55.9	56.9	56.1	56.1	50.2
absorp corr (T_{min}, T_{max})	0.801, 0.912	0.720, 0.886	0.450, 0.545	0.709, 0.760	0.733, 0.965
total no. of reflns	80 087	38 177	55 034	45 818	48 876
no. of indep reflns (R_{int})	6271 (0.059)	8249 (0.050)	6207 (0.032)	7081 (0.031)	11 134 (0.048)
residuals (refined on F^2, all data): R_1; wR_2[a]	0.049; 0.062	0.073; 0.106	0.031; 0.061	0.034; 0.044	0.065; 0.063
GOF	1.02	1.03	1.07	1.07	1.02
no. of observations [$I > 2\sigma(I)$]	4604	5958	5496	5874	8119
residuals (refined on F): R_1; wR_2[a]	0.027; 0.054	0.045; 0.095	0.024; 0.059	0.021; 0.040	0.034; 0.055

[a] $R_1 = \sum||F_o| - |F_c||/\sum|F_o|$. $wR_2 = [\sum w(F_o^2 - F_c^2)^2/\sum w(F_o^2)^2]^{1/2}$.

2.47 (1H, m, −CH_2− of DACH), 2.21, (6H, br s, N-(CH_3)$_2$), 1.90 (3H, m, −CH_2− of DACH), 1.61 (1H, t, J = 10 Hz, −CH_2− of DACH), 1.43 (9H, s, *t*-Bu), 1.28 (9H, s, *t*-Bu), 1.24 (1H, m, −CH_2− of DACH), −0.15 (3H, s, In-CH_3), −0.35 (3H, s, In−CH_3). ^{13}C{^{1}H} NMR (75 MHz, $CDCl_3$): δ 163.9, 138.3, 133.0, 124.3, 123.7, 122.8, 66.8, 58.1, 53.8, 35.4, 33.9, 32.6, 32.0, 29.7, 25.2, 24.8, 21.5, −7.0, −7.2. EI-LRMS (*m*/*z*): 504. Anal. Calcd (found) for $C_{25}H_{45}InN_2O$: C, 59.50 (59.36); H, 8.90 (8.88); N, 5.55 (5.50).

(NN$_H$O)InBr$_2$ (4). A solution of K(NN$_H$O) (0.112 g, 0.29 mmol) in 5 mL of THF was added dropwise to a solution of $InBr_3$ (0.105 g, 0.29 mmol) in 5 mL of THF. The reaction was stirred at room temperature for 2 h, and the formation of KBr was observed. The salt was removed by filtration through glass filter paper, the remaining yellow-orange solution was evaporated to dryness, and the residue was dried 2 h *in vacuo*. Complex **4** was obtained as a yellow crystalline solid (0.155 g; 83% yield). Suitable crystals for X-ray diffraction were grown by slow diffusion of pentane in a CH_2Cl_2 solution of complex **4**. ^{1}H NMR (400 MHz, CD_2Cl_2): δ 7.27 (1H, d, J = 3 Hz, Ar*H*), 6.88 (1H, d, J = 3 Hz, Ar*H*), 4.15 (1H, triplet, R_2N-C*H*-CH_2), 4.06 (1H, d, J = 12 Hz, NH-CH_2-Ar), 2.71 (3H, s, N(*Me*)(Me)), 2.60 (2H, m, C*H*NH and C*H*NMe$_2$), 2.48 (3H, s, N(Me)(*Me*)), 1.95 (6H, m, −CH_2− of DACH), 1.43 (9H, s, *t*-Bu), 1.28 (11 H, s, *t*-Bu and m, CH_2 of DACH). ^{13}C{^{1}H} NMR (100.64 MHz, CD_2Cl_2): δ 163.5, 138.2, 136.8, 126.2, 125.9, 118.8, 53.4, 51.2, 38.3, 36.0, 34.5, 32.5, 31.7, 31.2, 30.4, 24.8, 24.7, 22.2, 27.7. EI-LRMS (*m*/*z*) [M$^+$] 634. Anal. Calcd (found) for $C_{25}H_{39}Br_2InN_2O$: C, 47.30 (47.29); H, 6.15 (6.13); N, 4.42 (4.41).

(NN$_H$O)InI$_2$ (5). A similar procedure to that for complex **4** was used using InI_3 (0.171 g, 0.34 mmol) and KNN$_H$O (0.130 g, 0.34 mmol). The reaction was stirred at room temperature for 2 h, and then KI formation was observed. The salt was removed by filtration through glass filter paper, and the remaining yellow solution was evaporated to dryness. Complex **5** was obtained as a yellow powder (0.235 g; 95% yield). ^{1}H NMR (400 MHz, CD_2Cl_2): δ 7.26 (1H, d, J = 3 Hz, Ar*H*), 6.88 (1H, d, J = 3 Hz, Ar*H*), 4.13 (1H, t, J = 12 Hz, R_2N-C*H*-CH_2), 3.97 (1H, d, J = 15 Hz, NH-CH_2-Ar), 2.78 (2H, m, NC*H* of DACH), 2.62 (3H, s, NMe*Me*), 2.46, (3H, s, N*Me*Me), 1.91 (4H, m, −CH_2− of DACH), 1.44 (9H, s, *t*-Bu), 1,33 (2H, m, −CH_2− of DACH), 1.28 (9H, s, *t*-Bu), 1.27 (2H, m, −CH_2− of DACH. ^{13}C{^{1}H} NMR (100.64 MHz, CD_2Cl_2): δ 163.5, 139.9, 136.9, 126.0, 125.9, 118.8, 53.5, 51.2, 38.5, 36.2, 34.5, 32.5, 31.8, 31.3, 30.6, 24.9, 24.8, 22.1, 21.8. EI-LRMS (*m*/*z*) [M$^+$]: 728. Anal. Calcd (found) for $C_{25}H_{39}I_2InN_2O$: C, 41.20 (41.15); H, 5.36 (5.35); N, 3.84 (3.81).

{[(NN$_H$O)InBr]$_2$(μ-Br)(μ-OEt)} (7). A 25 mL round-bottom flask was charged with complex **4** (0.100 g, 0.16 mmol) dissolved in 5 mL of toluene. A solution of NaOEt (0.011 g, 0.16 mmol) in 5 mL of toluene was added dropwise to this mixture. After stirring the reaction mixture for 2 h at room temperature, NaBr formation was observed. The salt was removed by filtration through glass filter paper, and the remaining yellow solution was evaporated to dryness. The residue was washed with pentane and dried for 2 h *in vacuo* to yield complex **7** as a white powder (0.071 g, 70% yield). ^{1}H NMR (400 MHz, CD_2Cl_2): δ 7.20 (1H, d, J = 4 Hz, Ar*H*), 6.80 (1H, d, J = 3 Hz, Ar*H*), 4.81 (1H, d, J = 12 Hz, HN-C*H*H-Ar), 4.40 (m, 1H, OC*H*HMe), 4.19 (1H, m, OCH*H*Me), 3.72 (1H, d, J = 12 Hz, NH-CH*H*-Ar), 2.55 (3H, s, N*Me*Me), 2.48 (2H, m, C*H*N(Me)$_2$ and C*H*NH), 1.89 (3H, s, NMe*Me*), 1.85 (4H, m, −CH_2− of DACH), 1.43 (9H, s, *t*-Bu), 1.41 (2H, t J = 8 Hz, OCH$_2$C*H*$_3$), 1.27 (11H, s, *t*-Bu and m, −CH_2− of DACH), 1.07 (2H, m, −CH_2− of DACH). ^{13}C{^{1}H} NMR (100.64 MHz, CD_2Cl_2): δ 163.3, 138.7, 136.7, 129.5, 125.8, 120.0, 67.4, 61.2, 50.6, 45.7, 38.1, 35.8, 34.3, 32.1, 30.3, 26.4, 25.4, 25.3, 22.4, 19.9. EI-LRMS (*m*/*z*): 554 (M$^+$ − In(NNO)(Br)2(OEt)), 634 (M$^+$ − In-(NNO)Br(OEt)). Anal. Calcd (found) for $C_{48}H_{83}Br_3In_2N_4O_3$: C, 46.70 (46.72); N, 4.50 (4.34); H, 6.70 (6.69).

{[(NN$_H$O)InI]$_2$(μ-I)(μ-OEt)} (8). The same procedure to prepare complex **7** was followed using complex **5** (0.080 g, 0.11 mmol) dissolved in 5 mL of toluene and NaOEt (0.008 g, 0.11 mmol) in 5 mL of toluene. The reaction was stirred at room temperature for 12 h, and then NaI formation was observed. The salt was eliminated by filtration through glass filter paper, and the yellow solution was evaporated to dryness. The residue was washed with pentane, and **8** was obtained as a white powder, which was dried for 2 h *in vacuo* (0.051 mg; 68% yield). ^{1}H NMR (400 MHz, CD_2Cl_2): δ 7.22 (1H, d, J = 4 Hz, Ar*H*), 6.80 (1H, d, J = 3 Hz, Ar*H*), 4.84 (1H, d, J = 12 Hz, HN-C*H*H-Ar), 4.40 (m, 1H, OC*H*HMe). 4.21 (1H, m, OCH*H*Me), 3.75 (1H, d, J = 12 Hz, NH-CH*H*-Ar), 3.43 (1H, d, J = 12 Hz, C*H*NH), 2.66 (2H, m, −CH_2− of DACH), 2.56 (3H, s, N*Me*Me), 2.48, (1H, m,

C*H*N(Me)$_2$), 1.92 (3H, s, NMe*Me*), 1.83 (2H, m, −C*H*$_2$− of DACH), 1.44 (9H, s, *t*-Bu), 1.41 (2H, t J = 8 Hz, OCH$_2$C*H*$_3$), 1.28 (11H, s, *t*-Bu and m, −C*H*$_2$− of DACH), 1.14 (2H, m, −C*H*$_2$− of DACH). ^{13}C{^{1}H} NMR (100.64 MHz, CD_2Cl_2): δ 163.2, 138.9, 136.7, 126.8, 124.5, 119.9, 67.3, 62.0, 50.3, 46.0, 38.1, 35.7, 34.3, 32.2, 30.3, 26.2, 25.5, 26.3, 22.7, 19.6. EI-LRMS (m/z) 602 (M^+ − In(NNO)(I)2(OEt)), 728 (M^+ − In(NNO)I-(OEt)). Anal. Calcd (found) for $C_{48}H_{83}I_3In_2N_4O_3$: C, 41.91 (41.92); H, 6.03 (6.05); N, 4.10 (4.12).

[(NN$_H$O)InI(*μ*-OH)]$_2$ (10). Complex **8** was removed from the inert atmosphere and exposed to moist air for 24 h, to yield the air- and moisture-stable *μ*-OH dinuclear complex **10** in quantitative yield. Suitable crystals for X-ray diffraction were grown by slow diffusion of Et_2O in a CH_2Cl_2 solution of complex **10**. ^{1}H NMR (300 MHz, $CDCl_3$): δ 7.23 (1H, d, J = 3 Hz, Ar), 6.78 (1H, d, J = 3 Hz, Ar), 4.77 (1H, d, J = 15 Hz, NC*H*HAr), 3.87 (1H, b, OH), 3.73 (1H, d, J = 6 Hz, NCH*H*Ar), 3.37 (1H, d, J = 9 Hz, C*H*NH), 2.68 (1H, m C*H*NMe$_2$), 2.54 (3H, s, N*Me*Me) 2.20 (3H, m, C*H*$_2$ of DACH), 1.93 (3H, s, NMe*Me*), 1.81 (2H, m, C*H*$_2$ of DACH), 1.58 (2H, m, C*H*$_2$ of DACH), 1.47 (9H, s, *t*-Bu), 1.27 (9H, s, *t*-Bu), 1.08 (2H, m, C*H*$_2$ of DACH). ^{13}C{^{1}H} NMR (100 MHz, $CDCl_3$): δ 164.2, 139.8, 137.8, 127.3, 125.1, 121.2, 65.9, 53.1, 51.9, 51.2, 44.3, 38.7, 36.2, 34.9, 32.7, 31.6, 31.4, 31.2, 25.5, 25.4, 22.1. Anal. Calcd (found) for $C_{54}H_{100}N_4O_6In_2I_2$: C, 46.70 (46.32); H, 7.19 (7.18), N, 4.10 (4.11).

DFT Calculations. [42] The Amsterdam Density Functional (ADF) package (version ADF2009.01)[43,44] was used to do geometry optimizations on Cartesian coordinates for full molecules or model complexes. All structures were optimized in the gas phase starting with geometries obtained from the X-ray crystal structures. These optimized geometries were used as a starting point for calculations using the COSMO model for the appropriate solvent. The free energies for the pyridine-adduct formation of the halide complexes were calculated from gas-phase optimizations. For the indium and the halide atoms, standard triple-ζ STA basis sets from the ZORA ADF database TZP (no frozen cores) were employed. The local density approximation (LDA) by Becke−Perdew was used together with the exchange and correlation corrections that are employed by default by the ADF2009.01 program suite. Calculations for all complexes were carried out using the scalar spin−orbit relativistic formalism.

Acknowledgment. The authors thank UBC, NSERC, CFI, and BCKDF for funding and Chua Chong Yan for the synthesis of starting materials. P.L.D. thanks UCLA and the Sloan Foundation for support.

Supporting Information Available: Computational Details. This material is available free of charge via the Internet at http://pubs.acs.org.